



Article

# Composite Plastic Hybrid for Automotive Front Bumper Beam

Shada Bennbaia <sup>1</sup>, Elsadig Mahdi <sup>1</sup>, Galal Abdella <sup>1</sup> and Aamir Dean <sup>2,\*</sup>

<sup>1</sup> Department of Mechanical and Industrial Engineering, College of Engineering, Qatar University, Doha P.O. Box 2713, Qatar

<sup>2</sup> School of Civil Engineering, College of Engineering, Sudan University of Science and Technology, Khartoum P.O. Box 72, Sudan

\* Correspondence: a.dean@sustech.edu; Tel.: +249-(0)-155144366

**Abstract:** The bumper beam is a crucial component of the automobile bumper system, responsible for absorbing impact energy and enhancing the safety of passengers during collisions. This paper presents the design and experimental analysis of a 3D-printed composite–plastic hybrid light structure, designed as a collapsible energy absorber. Exploratory testing was conducted using low-impact tests to investigate the failure mechanism and energy absorption capacity of a spiral structure. The design process involved optimizing the spiral diameter by testing specimens with varying diameters between 0.5 cm and 2.5 cm, while keeping other geometric parameters constant. The study employed three types of 3D composite structures, including printed thermoplastic, printed thermoplastic reinforced with Kevlar fiber composite, and printed thermoplastic filled with foam. The thermoplastic–foam composite with nine spirals (diameter = 0.97 cm) yielded the best results. The new design demonstrated high energy absorption capacity and a controlled and progressive failure mechanism, making it a suitable candidate for energy absorption applications.

**Keywords:** crashworthiness; energy absorption capability; failures mechanism; bumper; spiral structure; composite; plastic; automotive



**Citation:** Bennbaia, S.; Mahdi, E.; Abdella, G.; Dean, A. Composite Plastic Hybrid for Automotive Front Bumper Beam. *J. Compos. Sci.* **2023**, *7*, 162. <https://doi.org/10.3390/jcs7040162>

Academic Editor: Francesco Tornabene

Received: 20 February 2023

Revised: 31 March 2023

Accepted: 7 April 2023

Published: 12 April 2023



**Copyright:** © 2023 by the authors. Licensee MDPI, Basel, Switzerland. This article is an open access article distributed under the terms and conditions of the Creative Commons Attribution (CC BY) license (<https://creativecommons.org/licenses/by/4.0/>).

## 1. Introduction

Frontal collisions are a leading cause of death and injury in road accidents. As such, researchers in crashworthiness have been focusing on reducing the occurrence of such accidents. According to the World Health Organization (WHO), road accidents are the primary cause of death for young adults and children between the ages of 5 and 29 [1]. Given this alarming statistic, the development of automotive safety systems has become a critical area of research. Crashworthiness refers to a vehicle's ability to absorb energy and provide adequate space for passengers to survive in the event of an accident. Therefore, the development of efficient energy absorption systems can significantly enhance the crashworthiness of cars [2–7]. In recent years, numerous studies have explored ways to improve the crashworthiness of vehicles, including the development of advanced materials and structures. Innovative energy absorption systems have also been designed to mitigate the effects of frontal collisions. These systems absorb the impact energy and dissipate it efficiently to prevent excessive deformation of the passenger compartment, while providing adequate survival space for passengers in the event of an accident. Consequently, the development of more efficient energy absorption systems can significantly enhance vehicle safety on the road. One crucial automotive component that endures accidents and impact stresses is the frontal bumper system [8–16]. As illustrated in Figure 1, this system comprises three key elements: the bumper beam, the absorber, and the fascia [17–19]. Lightweight materials have garnered significant attention in automotive applications, primarily due to the trend of replacing heavy parts to conserve fuel and reduce carbon footprint [20–33]. However, it is worth noting that the energy required to propel a vehicle is more than ten

times the energy used in the manufacturing process [34]. Therefore, developing eco-friendly cars is crucial, regardless of the energy consumed in producing lightweight materials.

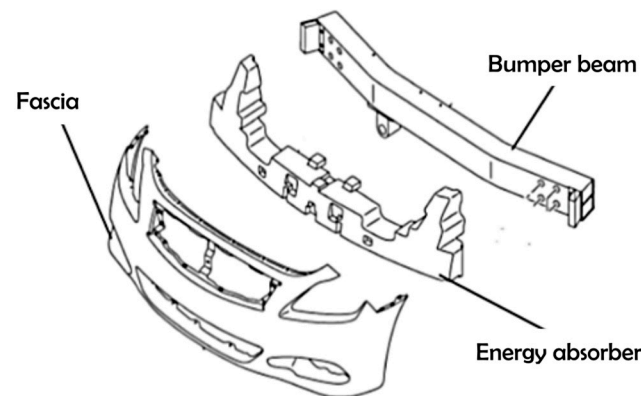


**Figure 1.** Standard bumper system [17].

Abrupt acceleration, which refers to rapid changes in velocity, is a common occurrence in vehicular crashes. However, the human body's ability to withstand such acceleration is limited, and exceeding these limits can result in severe injury or even death. Therefore, understanding the extent to which humans can tolerate such acceleration is essential in determining the necessary safety features and structural elements required to protect occupants in foreseeable crashes [35–39]. By knowing the crash environment and the limits of human tolerance to acceleration, designers can set crashworthiness design requirements that will effectively safeguard passengers in a variety of collision scenarios. For instance, if the crashworthiness design requirements are not set to adequately protect passengers in a high-speed collision, the vehicle's occupants may suffer severe injuries due to the abrupt acceleration. Conversely, if the requirements are set too high, the vehicle's weight and cost may increase excessively, which can be detrimental to the overall performance and affordability of the vehicle. Since this study focuses on automobile impact crashes, we consider the acceleration tolerance limit in the  $+G_x$  and  $-G_x$  directions, which is 45 G. Table 1 provides a summary of estimates of human tolerance in all axes. The bumper beam is the key structure absorbing the kinetic energy from a high-impact collision [17,40]. Additionally, it provides bending resistance in a low-impact collision [17,41,42]. The function of the bumper beam is to absorb the impact of collision energy in a controlled way before the energy is transferred to the passengers. Many studies have been conducted on thin-walled structures to determine their energy absorption capabilities. Common examples of thin-walled structures studied include square tubes, circular tubes, sandwich plates, and honeycombs [17]. Traditionally, steel has been the most common material used to make bumper beams due to its strength and durability. However, in the mid-1980s, polymer composite materials were introduced as an alternative to traditional materials such as metal, plastic, and aluminum. Polymer composites offer several advantages over conventional materials. One of the most significant benefits is their weight reduction [22]. In fact, polymer composites can offer up to 30% less weight than steel without sacrificing the bumper beam's bending strength [8,20,43]. This reduction in weight can have a positive impact on the vehicle's fuel efficiency and handling. In addition, it is easier to produce complex shapes from polymer composites, allowing designers to create more aerodynamic and stylish bumpers while maintaining their effectiveness [44,45]. Overall, the use of polymer composite materials in bumper beams represents a significant advancement in automotive safety technology. With their weight reduction, high energy absorption capacity, and ability to produce complex shapes, polymer composites are an attractive alternative to traditional materials, and their use is likely to continue to grow in the future.

**Table 1.** Human tolerance limits of deceleration [2].

The Direction of the Accelerative Force	Tolerance Level
Headward (+Gz)	20–25 G
Tailward (−Gz)	15 G
Lateral Right (+Gy)	20 G
Lateral Left (−Gy)	20 G
Back to Chest (+Gx)	45 G
Chest to Back (−Gx)	45 G

Moreover, natural fiber composite has gained significant attention in recent years. These materials are composed of natural fibers, such as flax, hemp, or jute, embedded in a polymer matrix [20,34,46–53]. The combination of these materials offers several advantages over conventional materials, including low density, high stiffness, and specific strength. In particular, sheet molding compound (SMC) bumper beams have been developed using natural fiber composites. These bumper beams have been found to be effective in maximizing the elastic strain energy while minimizing the impact force, bumper beam deflection, and stress distribution. This is due to the excellent properties of natural fiber composites, which offer an optimal combination of high strength and low rigidity. The use of high-strength materials leads to good impact behavior, which is crucial for safety in the automotive industry. On the other hand, the use of materials with low Young's modulus leads to low rigidity, which is important for reducing weight and improving fuel efficiency [54].

There are several significant factors that affect the energy absorption capacity of bumper beams, including their shape, cross-section, thickness, rib, and material. The cross-section and thickness of the bumper beam play crucial roles in determining the amount of energy that can be absorbed during a collision. In addition, the presence of reinforcing ribs in the bumper beam can significantly increase its energy absorption capacity. The use of rib-reinforced beams has been found to be more effective in absorbing energy than foam-filled and empty square beams. Moreover, these strengthening ribs can enhance the overall stabilization and rigidity of the bumper structure, which can contribute to better performance in collision scenarios. Understanding the impact of these factors on the energy absorption of bumper beams is crucial in the design and development of safer and more effective vehicle bumpers [55,56].

According to a study by Zhang [57], tubes with graded thickness in the cross-section can increase the energy absorption under axial loading by up to 30–35%. In [58], it has been stated that a sheet with varying thickness improves crashworthiness. Moreover, functionally graded structures with changing wall thickness along the longitudinal direction offer sufficient absorption of crushing energy. A study by Zarei [59] showed that, for aluminum structures, the wall thickness should be between 0.5 and 3.5 cm to maximize specific energy absorption.

A study conducted by Sinha [60] investigated two major factors. The first is the internal absorbed energy by the bumper beams, which they found can be kept high using materials with a high modulus of elasticity and high yield strength. The second factor is plastic deformation, which should be eliminated as much as possible during a low-speed mode. They found that material M220 is the best for bumper beam manufacturing. By using this material, the maximum stress of the bumper is kept below the material's yield stress, and the maximum beam deformation is kept within an acceptable limit.

Overall, it can be seen that the energy absorption capabilities of spiral structures have not been investigated before. The present study investigated the dynamic impact test responses of the different spiral structure composites using drop-weight impact equipment at an energy level of 15 J. Three types of composite materials were produced. These are 3D-printed thermoplastic, 3D-printed thermoplastic covered with a Kevlar fiber composite, and 3D-printed thermoplastic plastic filled with foam. All the samples were wrapped with Kevlar to control the failure mechanism. Test characteristics and results, such as energy absorption and damage modes, were evaluated. It is worth mentioning that Kevlar

fiber composite was used due to its well-known excellent impact and abrasion resistance characteristics in comparison to other fiber composites [61,62]. Moreover, the foam was added to enhance the axial stiffness and stability of the proposed design [63].

## 2. Experimental Program and Settings

### 2.1. Material Selection

ABS thermoplastic was chosen for producing the various spiral structures using 3D printing techniques. Kevlar fiber and blue Styrofoam composites were added to the plastic structures to create different specimens. The Kevlar fiber was fixed using EL2 epoxy laminating resin and AT30 slow epoxy hardener with a 100-30 ratio, while the blue foam was fixed using paper glue. Kevlar was used as a wrap for all specimens.

### 2.2. Specimen Preparation

The geometry and dimensions of the models are shown in Figure 2, which illustrates the different spiral structures that were modeled using SOLIDWORKS software. The geometric parameters of each structure are provided in Table 2. A total of four different spiral structures were produced, and six samples of each structure were 3D printed using ABS thermoplastic, resulting in a total of 24 specimens arranged in three groups.

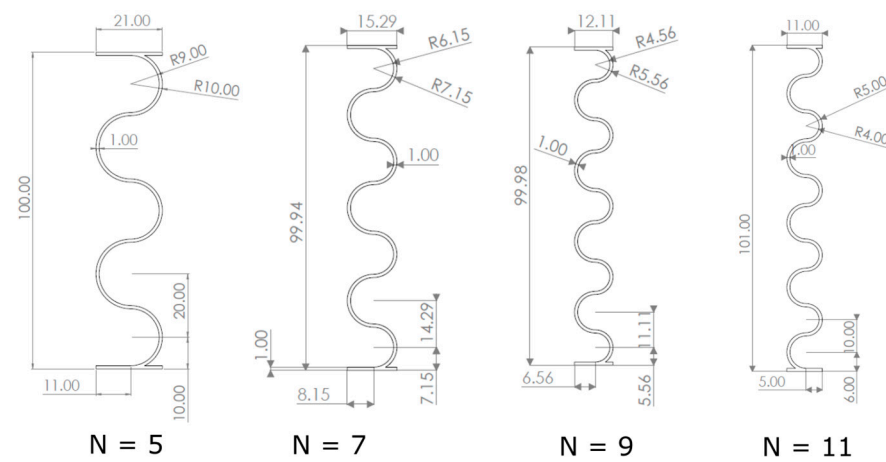


**Figure 2.** Printed models' geometry and dimensions (all dimensions are in mm).

**Table 2.** The geometric parameters of the specimens.

Number of Spirals (N)	Diameter (cm)	Height (cm)	Thickness (cm)
5	1.84	10	0.1
7	1.29	10	0.1
9	0.97	10	0.1
11	0.78	10	0.1

Kevlar fiber composite was added to the first group of samples by wrapping two layers on each side of the plastic specimen. Next, Styrofoam was used as a core for the second group; the foam was cut by a CNC machine based on the dimensions of the spiral structure and then glued to the structures with polyvinyl acetate. Finally, the third group material was 3D-printed thermoplastic, used as a control. Two layers of Kevlar composite were wrapped around each specimen to add some controllability to the failure mechanism during the dynamic impact test (see Figure 3a).

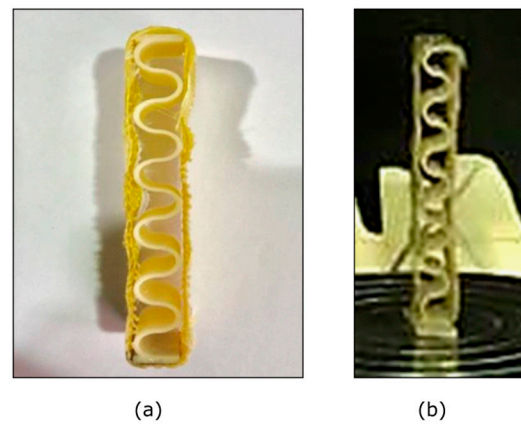


**Figure 3.** (a) Sample of the plastic specimens after adding Kevlar composite; (b) a specimen inside the low-impact test machine before the impact test.

### 2.3. Low-Velocity Impact (LVI)

LVI tests were carried out partially in accordance with the standardized test, ASTM D7136/D7136M [64], using the drop-weight impact testing machine from Imatek. The specimen was fixed vertically at the center of the base by a double-sided tape to prevent the samples from slipping (see Figure 3b).

Twenty-four impact tests were carried out. All impact conditions, such as the impactor geometry and mass, incident energy, and height of the impactor, were the same for all samples. The initial impact energy was set to 15 J (mass = 11.83 kg and velocity = 1.56 m/s) for all composite specimens. Force and displacement as a function of time and initial impact velocity were recorded by the machine's automatic data acquisition system. Acceleration, velocity, and energy were then automatically calculated. All impact tests were filmed using a digital high-speed video camera with 3000 frames per second for slow-motion analysis. In addition, pictures before and after the test were captured for all the specimens.

## 3. Results and Discussion

The impact response of each specimen was recorded as a function of time. The recorded parameters are (1) force, (2) displacement, and (3) acceleration. The following section is dedicated to showcasing and discussing the experimental results.

### 3.1. Impact Performance

Figure 4 shows the spiral hybrid composite structure's typical force versus displacement response. The initial drop in the load is a sign of crack initiation; a few fluctuations in the curves represent the propagation of cracks, resulting in stiffness degradation. The plots' peak force represents the load a structure can withstand before undergoing critical damage.

In case (A)  $N = 5$ , the Kevlar fiber composite has a very high peak force compared to plastic and blue foam composites; after a displacement of around 2 cm, the resistance of the composite started degrading, cracking down under the impactor. The plastic composite showed very low resistance to load and failed almost immediately. In case (B)  $N = 7$ , the blue foam composite has the highest peak force at around 2 cm displacement. The Kevlar fiber composite started failing at approximately 1 cm displacement with a peak force of less than 70 N than the Kevlar fiber composite. Cases (C)  $N = 9$  and (D)  $N = 11$  results are close; there is a sudden drop in the impact force response after peak force at around 2 cm displacement, and then the load oscillates as the structures fail down. Based on the force resistance stability, the blue foam composite performed better than the others, regardless of the number of spirals.

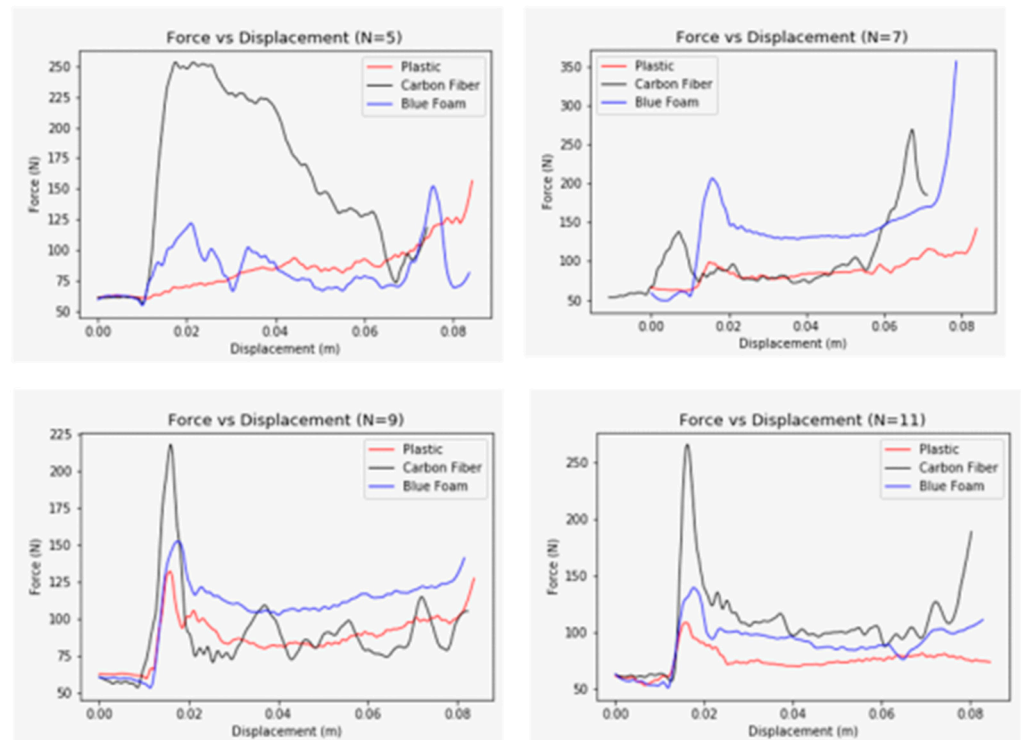


**Figure 4.** Experimental impact force–displacement response with different numbers of spirals (N).

Figure 5 shows the acceleration versus time response of the spiral hybrid composite structures. The best performance is when the acceleration values are stable at around  $0 \text{ m/s}^2$ . In cases (A), (B), (C), and (D), the blue foam composite has the best acceleration stability. Compared to the human acceleration tolerance limit ( $45 \text{ g}$ ), the highest acceleration in the plots shown in Figure 5 is around  $12.5 \text{ m/s}^2$ , equal to  $1.275 \text{ g}$ , which is perfectly safe for humans.

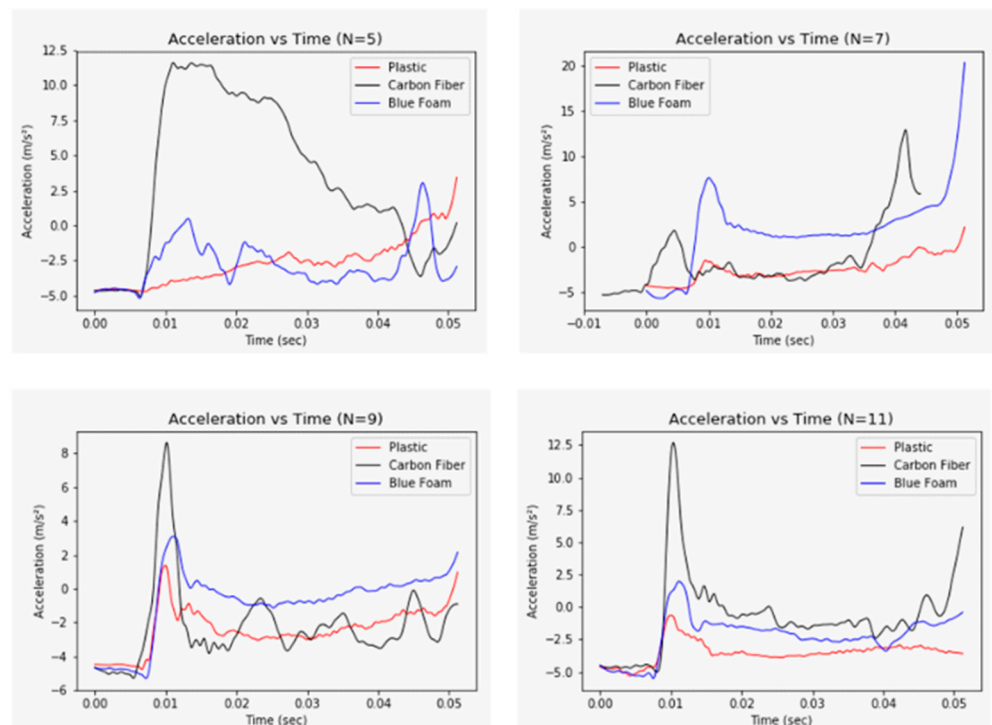


**Figure 5.** Experimental impact acceleration–time response with different number of spirals (N).

Figure 6 shows a chart representing the hybrid composites' energy absorption levels. The blue foam composite achieved the highest energy absorption level of 11.7 J when N = 5. The lower level was the plastic composite when N = 11 at 6.3 J. However, the performance based on the energy-to-weight ratio was different, as shown in Figure 7. The highest specific energy absorption of 1065 J/kg was achieved by the blue foam composite when the number of spirals was 9, and similar specific energy absorptions were achieved by the plastic composite when N = 5, 7, and 11 and by the blue foam composite when N = 11. The lower level was achieved by the Kevlar fiber when N = 9 at 482.6 J/kg.

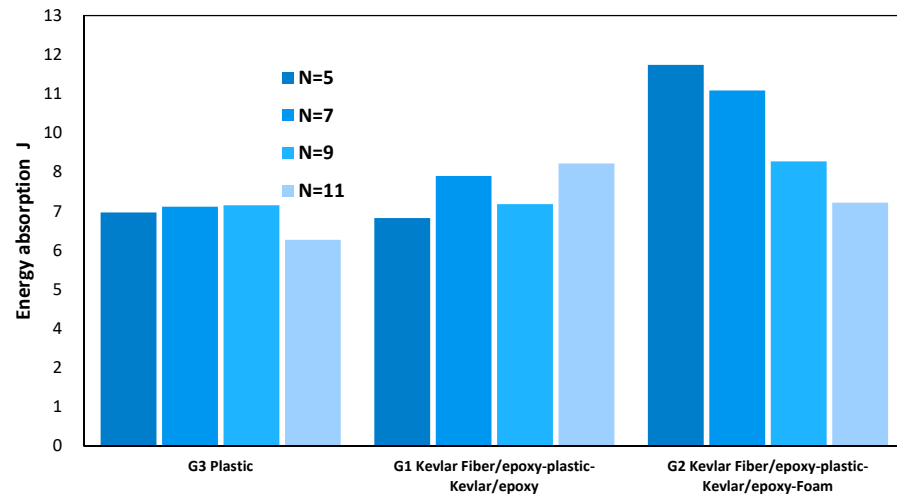


Figure 6. Energy absorption level of the three composites with different numbers of spirals (N).

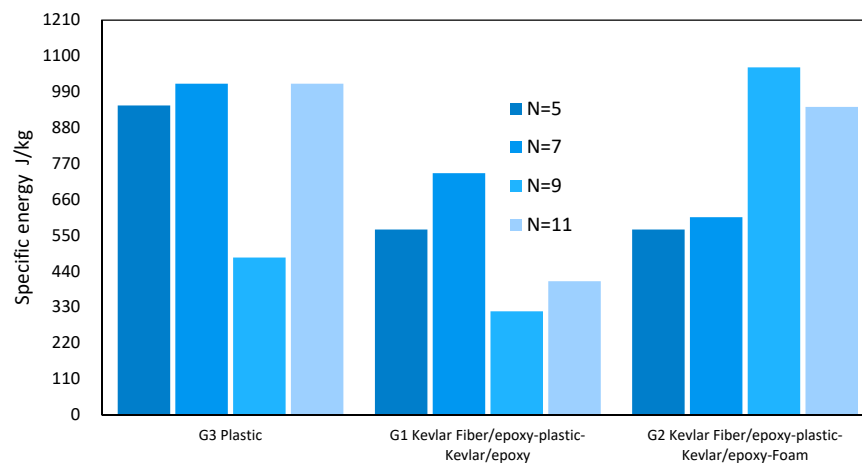


Figure 7. The specific energy level of the three composites with different numbers of spirals (N).

Based on the observations above, these hybrid composites achieve the best performance under dynamic impact: blue foam N = 9, Kevlar fiber N = 7, and plastic N = 11. The failure mechanism and structure analyses were conducted for these three composites using the videos recorded by a high-speed camera during the experiments.

### 3.2. Structure Recoverability

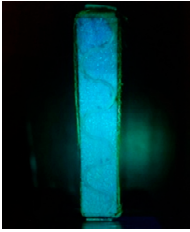
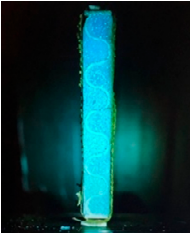
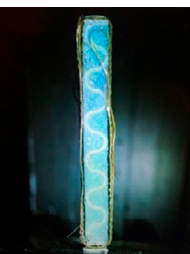
Table 3 shows the pictures of the specimens taken before and after each LVI test to evaluate the recoverability of the hybrid composites. All the Kevlar fiber composite structures fractured into pieces (8 to 12 pieces). The resin and epoxy hardener made the structure hard but brittle; thus, it cracked during failure. The plastic composites also have poor recoverability but are slightly better than Kevlar fiber. However, the blue foam composite structures have the best recoverability; as seen in the photos in Table 3,

all the plastic structures covered by the blue foam recovered without any breakage or critical damage.

**Table 3.** The examined structures before and after the LVI test.

Material	No. of Spirals	Sample Picture before the Test	Sample Picture after the Test
ABS Plastic	5		
ABS Plastic	7		
ABS Plastic	9		
ABS Plastic	11		
ABS Plastic and Kevlar Fiber	5		
ABS Plastic and Kevlar Fiber	7		

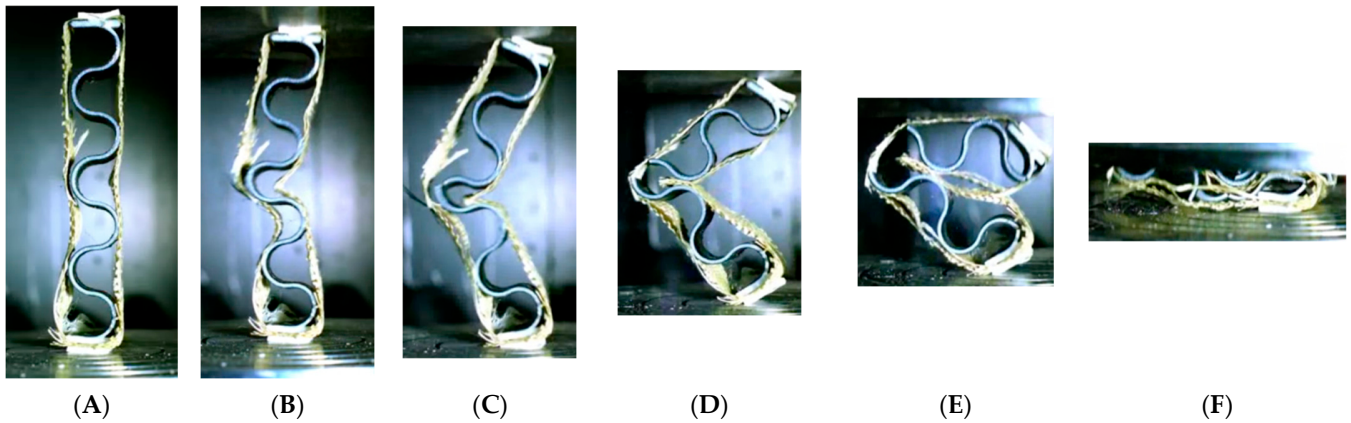
Table 3. Cont.

Material	No. of Spirals	Sample Picture before the Test	Sample Picture after the Test
ABS Plastic and Kevlar Fiber	9		
ABS Plastic and Kevlar Fiber	11		
ABS Plastic and Foam	5		
ABS Plastic and Foam	7		
ABS Plastic and Foam	9		
ABS Plastic and Foam	11		

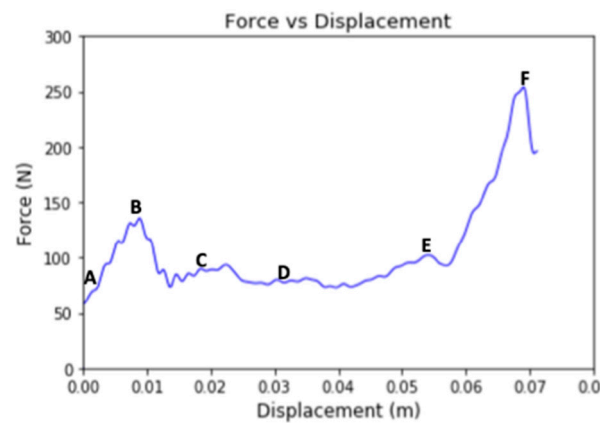
### 3.3. Structural Failure Analysis

Figure 8A shows the Kevlar fiber hybrid structure in the impact test machine. It can be seen that the Kevlar composite is fixed to the structure on the right side and not the left. Figure 8B shows that matrix cracking started; it is evident on the right side and not the other side, initiating local buckling at the bottom half on the right side where the Kevlar is

free to go inwards. In Figure 8C, as the compression progresses, the structure follows the Kevlar buckling pattern, and the global buckling of mode one happens in the middle of the structure. As the compression continues, it can be seen in Figure 8D that the structure fractured in the middle because of the increasing bending. As the top of the structure goes downward, multiple cracks at the spirals can be observed in Figure 8E. From the graph in Figure 9, the deceleration is almost zero in the areas represented by Figure 8C–E because there was no resistance as the structure bent down. However, at the end of the graph, the force reached its maximum value when the top part of the structure contacted the bottom part, in Figure 8F, due to increased resistance.



**Figure 8.** Kevlar fiber with  $N = 7$  specimen under the test. (A–F) retrace the failure process at different configuration (loading stage).



**Figure 9.** Experimental impact force–displacement response for Kevlar fiber with  $N = 7$ .

Figure 10A shows the blue foam hybrid structure in the impact test machine. It can be seen that the Kevlar composite is fixed on the right side and not on the left, similar to the specimen with the Kevlar fiber. Figure 10B shows that matrix cracking started to occur on the right side of the structure as global buckling happened. It can be seen that Kevlar is getting free and going outwards. In Figure 10C, the structure falls following the Kevlar buckling pattern as the compression continues. It can be seen in Figure 10D that the foam in the structure started to fracture in the middle because of the increasing bending. Figure 10C–E refer to the graph in Figure 11; it can be seen that the force applied is almost constant, which means the structure absorbs energy at a stable rate, meaning the deceleration is almost zero in this area. However, the force did not reach its maximum value at the end of the graph as the foam mass still resists the impactor, as shown in Figure 10F.

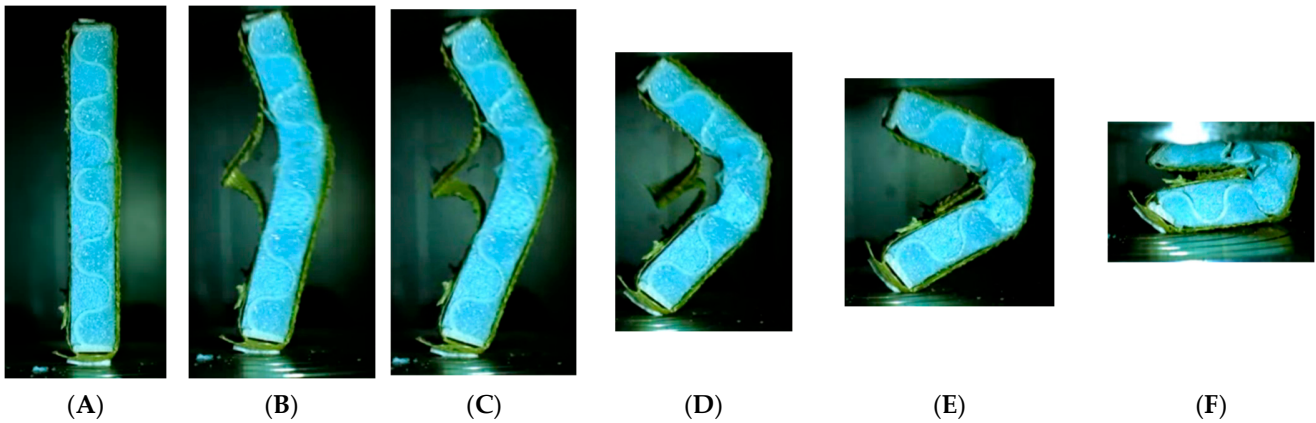


**Figure 10.** Blue foam with  $N = 9$  specimen under the test. (A–F) retrace the failure process at different configuration (loading stage).

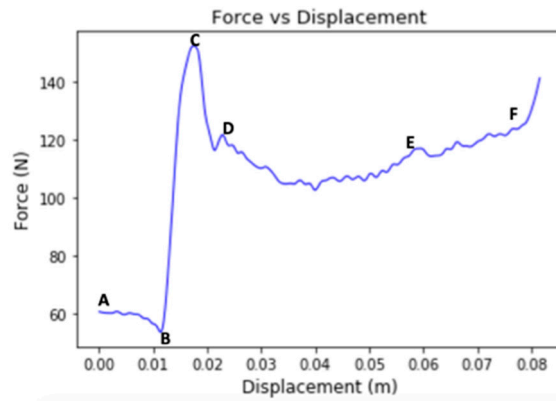


**Figure 11.** Experimental impact force–displacement response for blue foam with  $N = 9$ .

Figure 12A shows the plastic with the Kevlar composite hybrid structure in the impact test machine. In Figure 12B, a light matrix cracking starts as the Kevlar separates from the plastic. In Figure 12C, as the compression continues, the Kevlar separates from the structure’s right side while supporting the structure on the left side. Then, in Figure 12D, the structure fractures, and the 3D-printed plastic layers separate in the bending area. As the top of the structure goes downward, multiple cracks at the plastic spirals can be observed in Figure 12E. From the graph in Figure 13, it can be seen that the maximum force is around 110 N, which is much less than the other two structures. The force then drops down to about 71 N and keeps fluctuating in the areas represented by Figure 12C–E.

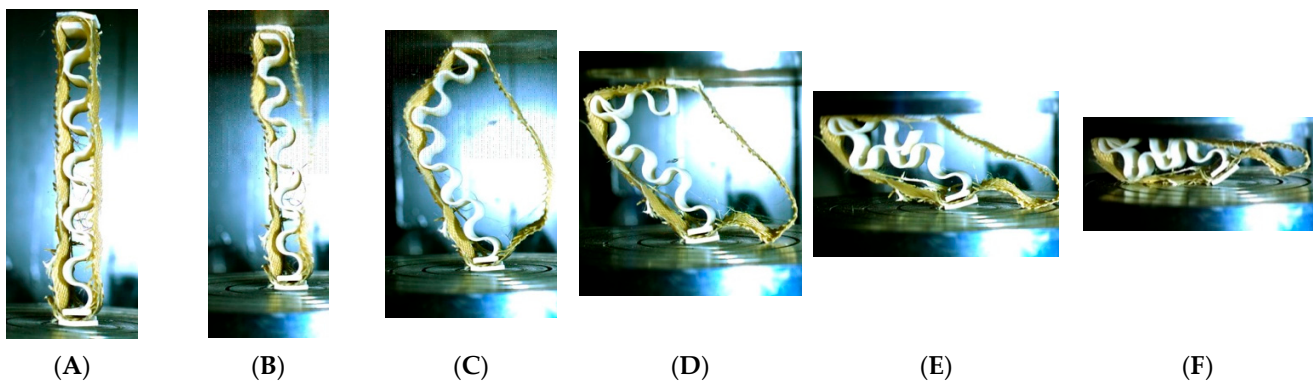


**Figure 12.** Plastic with  $N = 11$  specimen under the test. (A–F) retrace the failure process at different configuration (loading stage).

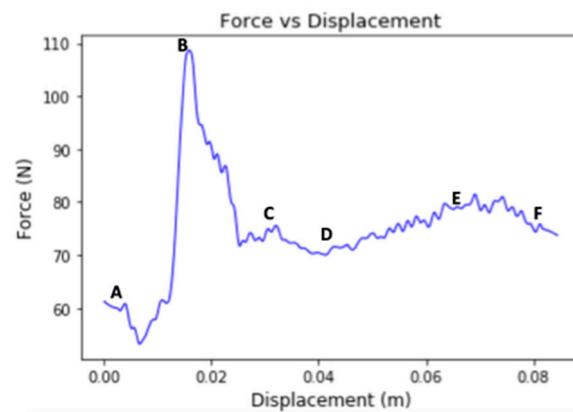


Figure 13. Experimental impact force–displacement response for plastic with N = 11.

For an in-depth understanding of the performance of the proposed design, the design should be investigated under fatigue loading conditions (see [65]). Furthermore, a virtual test rig should be built for a more thorough investigation. For this purpose, the following sophisticated models developed in [66–69] can be employed.

#### 4. Variability Analysis: Energy Absorption Versus Composition Type

One-way analysis of variance (ANOVA) is a statistical technique used to evaluate whether there are any significant differences between the means of two or more groups. Herein, ANOVA was used to estimate how the average energy absorption changed depending on the number of spirals and the composition type. To perform the ANOVA, the data were first divided into groups based on the number of spirals and the composition type. The average energy absorption for each group was then calculated and compared to see if there are any significant differences between them. In this analysis, more weight is given to the impact of the composition type, meaning that the effect of the composition type on energy absorption is considered to be more important than the effect of the number of spirals. Table 4 shows the settings of the two ANOVA tests.

Table 4. Energy absorption ANOVA settings.

Number of Spirals	Composition Type		
	Plastic	Kevlar Fiber	Foam
5	7.164	6.991	11.689
7	7.339	8.281	10.904
9	7.384	4.417	8.729
11	6.325	8.663	7.461

To continue, we formatted the problem as a hypothesis test, in which  $H_0$  states that there is no significant difference between the treatments and  $H_1$  states that at least one treatment has a significant impact. The level of significance ( $\alpha$ ) was set as equal to 0.1. Table 5 reports the ANOVA results.

Table 5. ANOVA results.

Source of Variability	DF	Sum of Square	Mean Square	F Statistic	p-Value
Spiral Number	3	8.0370	2.679	1.064	0.4315
Composition Type	2	18.380	9.191	3.650	0.0918
Error	6	15.106	2.518		
Total	11	41.524	3.775		

Since the  $p$ -value (0.0918)  $<$   $\alpha$  (0.1), the null hypothesis,  $H_0$ , is rejected (see Table 5). Therefore, some of the composition-type averages are considered as being not equal. In other words, the difference between the averages of composition type is large enough to be statistically significant. The results show that the chance of a type I error (rejecting a correct  $H_0$ ) is small (9.18%). The smaller the  $p$ -value, the more it supports  $H_1$ . The results show that the foam composition performs better than the other energy-absorbing types.

## 5. Conclusions

This paper presents the design and experimental analysis of a 3D composite plastic hybrid light structure as a collapsible energy absorber. Exploratory testing was conducted to investigate the failure mechanism and energy absorption capability of the spiral structure under impact. Moreover, a structure analysis was performed for the composite structures using high-speed camera videos recorded during the experiments. Based on the results, the hybrid composites achieved the best performance under dynamic impact: blue foam  $N = 9$ , Kevlar fiber  $N = 7$ , and plastic  $N = 11$ . The blue foam composite had the highest energy absorption level at 11.7 J, indicating that this hybrid structure absorbed approximately 75% of the impact energy.

**Author Contributions:** Conceptualization, S.B., E.M., G.A. and A.D.; methodology, S.B., E.M., G.A. and A.D.; software, S.B., E.M., G.A. and A.D.; validation, S.B., E.M., G.A. and A.D.; formal analysis, S.B., E.M., G.A. and A.D.; investigation, S.B., E.M., G.A. and A.D.; resources, S.B., E.M., G.A. and A.D.; data curation, S.B., E.M., G.A. and A.D.; writing—original draft preparation, S.B. and G.A.; writing—review and editing, E.M. and A.D.; visualization, S.B., E.M., G.A. and A.D.; supervision, E.M.; project administration, S.B., E.M. and G.A.; funding acquisition, E.M. All authors have read and agreed to the published version of the manuscript.

**Funding:** This research received no external funding.

**Data Availability Statement:** Data are unavailable due to privacy.

**Conflicts of Interest:** The authors declare no conflict of interest.

## References

1. World Health Organization. *Global Status Report on Road Safety 2018*; World Health Organization: Geneva, Switzerland, 2019.
2. Pathological Aspects and Associated Biodynamics in Aircraft Accident Investigation (Les Aspects Pathologiques et la Biodynamique Associee dans les Enquetes sur les Accidents D'aeronefs) (CD-ROM). Available online: <https://apps.dtic.mil/sti/citations/ADM001834> (accessed on 20 February 2023).
3. Alkhatib, F.; Mahdi, E.; Dean, A. Design and Evaluation of Hybrid Composite Plates for Ballistic Protection: Experimental and Numerical Investigations. *Polymers* **2021**, *13*, 1450. [[CrossRef](#)] [[PubMed](#)]
4. Alkhatib, F.; Mahdi, E.; Dean, A. Crushing response of CFRP and KFRP composite corrugated tubes to quasi-static slipping axial loading: Experimental investigation and numerical simulation. *Compos. Struct.* **2020**, *246*, 112370. [[CrossRef](#)]
5. Alkhatib, F.; Mahdi, E.; Dean, A. Development of composite double-hat energy absorber device subjected to traverser loads. *Compos. Struct.* **2020**, *240*, 112046. [[CrossRef](#)]
6. Mahdi, E.; Hamouda, A. Energy absorption capability of composite hexagonal ring systems. *Mater. Des.* **2012**, *34*, 201–210. [[CrossRef](#)]
7. Abdewi, E.F.; Sulaiman, S.; Hamouda, A.; Mahdi, E. Effect of geometry on the crushing behaviour of laminated corrugated composite tubes. *J. Mater. Process. Technol.* **2006**, *172*, 394–399. [[CrossRef](#)]
8. Mohammadi, H.; Ahmad, Z.; Mazlan, S.A.; Johari, M.A.F.; Siebert, G.; Petrú, M.; Kooloor, S.S.R. Lightweight Glass Fiber-Reinforced Polymer Composite for Automotive Bumper Applications: A Review. *Polymers* **2022**, *15*, 193. [[CrossRef](#)] [[PubMed](#)]
9. Godara, S.; Nagar, S.N. Analysis of frontal bumper beam of automobile vehicle by using carbon fiber composite material. *Mater. Today Proc.* **2020**, *26*, 2601–2607. [[CrossRef](#)]
10. Sun, G.; Wang, X.; Fang, J.; Pang, T.; Li, Q. Parallelized optimization design of bumper systems under multiple low-speed impact loads. *Thin-Walled Struct.* **2021**, *167*, 108197. [[CrossRef](#)]
11. Beyene, A.; Koricho, E.; Belingardi, G.; Martorana, B. Design and Manufacturing Issues in the Development of Lightweight Solution for a Vehicle Frontal Bumper. *Procedia Eng.* **2014**, *88*, 77–84. [[CrossRef](#)]
12. Wang, C.; Wang, W.; Zhao, W.; Wang, Y.; Zhou, G. Structure design and multi-objective optimization of a novel NPR bumper system. *Compos. Part B Eng.* **2018**, *153*, 78–96. [[CrossRef](#)]

13. Natarajan, N.; Joshi, P.; Tyagi, R. Design improvements of vehicle bumper for low speed impact. *Mater. Today Proc.* **2020**, *38*, 456–465. [CrossRef]
14. Lei, F.; Lv, X.; Fang, J.; Li, Q.; Sun, G. Nondeterministic multi-objective and multi-case discrete optimization of functionally-graded front-bumper structures for pedestrian protection. *Thin-Walled Struct.* **2021**, *167*, 106921. [CrossRef]
15. Belingardi, G.; Beyene, A.T.; Koricho, E.G.; Martorana, B. 12—Lightweight solutions for vehicle frontal bumper: Crash design and manufacturing issues. In *Dynamic Response and Failure of Composite Materials and Structures*; Woodhead Publishing: Cambridge, UK, 2017. [CrossRef]
16. Marzbanrad, J.; Alijanpour, M.; Kiasat, M.S. Design and analysis of an automotive bumper beam in low-speed frontal crashes. *Thin-Walled Struct.* **2009**, *47*, 902–911. [CrossRef]
17. Muhammad Nasiruddin, S.; Hambali, A.; Rosidah, J.; Widodo, W.S.; Ahmad, M.N. A Review of Energy Absorption of Automotive Bumper Beam. *Int. J. Appl. Eng. Res.* **2017**, *12*, 238–245.
18. Bohra, B.A.; Pawar, D.B. Comparative analysis of frontal car bumper during impact. *Int. J. Appl. Innov. Eng. Manag.* **2014**, *3*, 89–93.
19. Chege, A.; Kale, A.; Agrewale, M.R.B.; Vora, D.K.C. DESIGN AND DEVELOPMENT OF IMPACT ENERGY ABSORBING BUMPER. *Int. J. Sci. Eng. Res.* **2017**, *8*, 326–330.
20. Mahdi, E.; Ochoa, D.R.H.; Vaziri, A.; Dean, A.; Kucukvar, M. Khalasa date palm leaf fiber as a potential reinforcement for polymeric composite materials. *Compos. Struct.* **2020**, *265*, 113501. [CrossRef]
21. Dean, A.; Rolfes, R.; Grbic, N.; Hübner, S.; Behrens, B. A FEM-based virtual test-rig for hybrid metal-composites clinching joints. *Mater. Und Werkst.* **2019**, *50*, 973–986. [CrossRef]
22. Dean, A. *Material Modeling of Short Fiber Reinforced Polymeric Composites: Theory, Numerical Aspects, and Applications*; ISD, Institut für Statik und Dynamik: Hanover, Germany, 2017.
23. Dean, A.; Sahraee, S.; Reinoso, J.; Rolfes, R. Finite deformation model for short fiber reinforced composites: Application to hybrid metal-composite clinching joints. *Compos. Struct.* **2016**, *151*, 162–171. [CrossRef]
24. Gerendt, C.; Dean, A.; Mahrholz, T.; Englisch, N.; Krause, S.; Rolfes, R. On the progressive fatigue failure of mechanical composite joints: Numerical simulation and experimental validation. *Compos. Struct.* **2020**, *248*, 112488. [CrossRef]
25. Wang, B.; Zhang, Z.; Xu, G.; Zeng, X.; Hu, W.; Matsubae, K. Wrought and cast aluminum flows in China in the context of electric vehicle diffusion and automotive lightweighting. *Res. Conserv. Recycl.* **2023**, *191*, 106877. [CrossRef]
26. Gonçalves, M.; Monteiro, H.; Iten, M. Life Cycle Assessment studies on lightweight materials for automotive applications—An overview. *Energy Rep.* **2022**, *8*, 338–345. [CrossRef]
27. Ramasubramanian, S.; Tennis, K. Lightweight material for weight reductions in an automotive suspension part lower link. *Mater. Today Proc.* **2023**, in press. [CrossRef]
28. Ganesarajan, D.; Simon, L.; Tamrakar, S.; Kiziltas, A.; Mielewski, D.; Behabtu, N.; Lenges, C. Hybrid composites with engineered polysaccharides for automotive lightweight. *Compos. Part C Open Access* **2021**, *7*, 100222. [CrossRef]
29. Gardie, E.; Paramasivam, V.; Dubale, H.; Chekol, E.T.; Selvaraj, S.K. Numerical analysis of reinforced carbon fiber composite material for lightweight automotive wheel application. *Mater. Today Proc.* **2021**, *46*, 7369–7374. [CrossRef]
30. Wegmann, S.; Rytka, C.; Diaz-Rodenas, M.; Werlen, V.; Schneeberger, C.; Ermanni, P.; Caglar, B.; Gomez, C.; Michaud, V. A life cycle analysis of novel lightweight composite processes: Reducing the environmental footprint of automotive structures. *J. Clean. Prod.* **2021**, *330*, 129808. [CrossRef]
31. Zhang, W.; Xu, J. Advanced lightweight materials for Automobiles: A review. *Mater. Des.* **2022**, *221*, 110994. [CrossRef]
32. Junk, S.; Rothe, N. Lightweight design of automotive components using generative design with fiber-reinforced additive manufacturing. *Procedia CIRP* **2022**, *109*, 119–124. [CrossRef]
33. Liu, B.; Yang, J.; Zhang, X.; Yang, Q.; Zhang, J.; Li, X. Development and application of magnesium alloy parts for automotive OEMs: A review. *J. Magnes. Alloy.* **2023**, *11*, 15–47. [CrossRef]
34. McCrum, N.G.; Buckley, C.P.; Bucknall, C.B.; McCrum, N.G.; Buckley, C.P.; Bucknall, C.B. *Principles of Polymer Engineering*, 2nd ed.; Oxford University Press: Oxford, NY, USA, 1997.
35. Snyder, R.G. Human Impact Tolerance. *SAE Trans.* **1970**, *79*, 1375–1452.
36. Chou, C.C.; Bois, P.D.; Fileta, B.B.; Khalil, T.B.; King, A.I.; Mahmood, H.F.; Mertz, H.J.; Wismans, J. Vehicle Crashworthiness and Occupant Protection. Available online: [https://roadsafellc.com/NCHRP22-24/Literature/Papers/Vehicle%20Crashworthiness%20and%20Occupant%20Protection\(Book\).pdf](https://roadsafellc.com/NCHRP22-24/Literature/Papers/Vehicle%20Crashworthiness%20and%20Occupant%20Protection(Book).pdf) (accessed on 28 March 2023).
37. Prasad, P. Biomechanical Basis for Injury Criteria Used in Crashworthiness Regulations: ‘Bertil Aldman Award’ Lecture. 1999. Available online: <https://www.semanticscholar.org/paper/BIOMECHANICAL-BASIS-FOR-INJURY-CRITERIA-USED-IN-Prasad/986c44c84ab9b2b78c3f61362b3ab052a31aa239> (accessed on 28 March 2023).
38. Shopping for Safety: Providing Consumer Automotive Safety Information. *Transp. Res. Board Spec. Rep.* 1996. Available online: <https://trid.trb.org/View/462475> (accessed on 28 March 2023).
39. Zini, G. *Reduction of Crash Severity Through In-Vehicle Systems (IVS) Speed Control*; University of Buenos Aires: Buenos Aires, Argentina, 2005.

40. Raju, K.; Rao, K.N.; Santhosh, T.R.; Krupa, C.S. *Bumper Beams is Absorbing the Bulk of Energy and Providing Protection to the Rest of the Vehicle*; St. Martins Engineering College: Secunderabad, India, 2015.
41. Cheon, S.S.; Choi, J.H.; Gil Lee, D. Development of the composite bumper beam for passenger cars. *Compos. Struct.* **1995**, *32*, 491–499. [[CrossRef](#)]
42. Du, B.; Li, Q.; Zheng, C.; Wang, S.; Gao, C.; Chen, L. Application of Lightweight Structure in Automobile Bumper Beam: A Review. *Materials* **2023**, *16*, 967. [[CrossRef](#)] [[PubMed](#)]
43. Davoodi, M.; Sapuan, M.S.; Ahmad, D.; Aidy, A.; Ali, A.; Jonoobi, M. Concept selection of car bumper beam with developed hybrid bio-composite material. *Mater. Des.* **2011**, *32*, 4857–4865. [[CrossRef](#)]
44. Hsissou, R.; Seghiri, R.; Benzekri, Z.; Hilali, M.; Rafik, M.; Elharfi, A. Polymer composite materials: A comprehensive review. *Compos. Struct.* **2021**, *262*, 113640. [[CrossRef](#)]
45. Egorov, S.A.; Tarasova, T.V.; Terekhina, S.M. Production technology for polymeric composite materials by additive manufacturing methods. *IOP Conf. Ser. Mater. Sci. Eng.* **2020**, *971*, 022006. [[CrossRef](#)]
46. Mahdi, E.; Dean, A. The Effect of Filler Content on the Tensile Behavior of Polypropylene/Cotton Fiber and poly(vinyl chloride)/Cotton Fiber Composites. *Materials* **2020**, *13*, 753. [[CrossRef](#)] [[PubMed](#)]
47. Chichane, A.; Boujmal, R.; El Barkany, A. Bio-composites and bio-hybrid composites reinforced with natural fibers: Review. *Mater. Today Proc.* **2023**, *72*, 3471–3479. [[CrossRef](#)]
48. Bi, X.; Huang, R. 3D printing of natural fiber and composites: A state-of-the-art review. *Mater. Des.* **2022**, *222*, 111065. [[CrossRef](#)]
49. Ismail, S.O.; Akpan, E.; Dhakal, H.N. Review on natural plant fibres and their hybrid composites for structural applications: Recent trends and future perspectives. *Compos. Part C Open Access* **2022**, *9*, 100322. [[CrossRef](#)]
50. Santhosh, N.; Selvam, S.; Reghu, R.; Sundaran, J.; Mathew, B.C.; Palanisamy, S. Mechanical properties studies on rubber composites reinforced with Acacia Caesia fibre. *Mater. Today Proc.* **2023**, *72*, 3172–3176. [[CrossRef](#)]
51. Zaghoul, M.Y.M.; Zaghoul, M.M.Y.; Zaghoul, M.M.Y. Developments in polyester composite materials—An in-depth review on natural fibres and nano fillers. *Compos. Struct.* **2021**, *278*, 114698. [[CrossRef](#)]
52. Dun, M.; Fu, H.; Hao, J.; Shan, W.; Wang, W. Tailoring flexible interphases in bamboo fiber-reinforced linear low-density polyethylene composites. *Compos. Part A Appl. Sci. Manuf.* **2021**, *150*, 106606. [[CrossRef](#)]
53. Karthi, N.; Kumaresan, K.; Sathish, S.; Gokulkumar, S.; Prabhu, L.; Vigneshkumar, N. An overview: Natural fiber reinforced hybrid composites, chemical treatments and application areas. *Mater. Today Proc.* **2019**, *27*, 2828–2834. [[CrossRef](#)]
54. Kim, J.-W.; Kim, H.-S.; Lee, D.-G. Manufacturing and Characterization of Glass Fiber/Polypropylene Prepreg for Automotive Bumper Beam. *J. Comput. Theor. Nanosci.* **2015**, *12*, 842–846. [[CrossRef](#)]
55. Tarlochan, F.; Hamouda, A.M.S.; Mahdi, E.; Sahari, B.B. Composite sandwich structures for crashworthiness applications. *Proc. Inst. Mech. Eng. Part L J. Mater. Des. Appl.* **2007**, *221*, 121–130. [[CrossRef](#)]
56. Hosseinzadeh, R.; Shokrieh, M.M.; Lessard, L.B. Parametric study of automotive composite bumper beams subjected to low-velocity impacts. *Compos. Struct.* **2005**, *68*, 419–427. [[CrossRef](#)]
57. Zhang, Z.; Liu, S.; Tang, Z. Design optimization of cross-sectional configuration of rib-reinforced thin-walled beam. *Thin-Walled Struct.* **2009**, *47*, 868–878. [[CrossRef](#)]
58. Zhang, X.; Wen, Z.; Zhang, H. Axial crushing and optimal design of square tubes with graded thickness. *Thin-Walled Struct.* **2014**, *84*, 263–274. [[CrossRef](#)]
59. Zarei, H.; Kröger, M. Bending behavior of empty and foam-filled beams: Structural optimization. *Int. J. Impact Eng.* **2008**, *35*, 521–529. [[CrossRef](#)]
60. Sinha, A.; Yadav, K.; Khurana, R.S. *Design of Bumper Beam Structure for Pedestrian Protection and Low Speed Bumper Impact(ECE-R42)*; SAE Technical Paper 2016-01-1335; SAE International: Warrendale, PA, USA, 2016. [[CrossRef](#)]
61. Singh, T.J.; Samanta, S. Characterization of Kevlar Fiber and Its Composites: A Review. *Mater. Today Proc.* **2015**, *2*, 1381–1387. [[CrossRef](#)]
62. Rajesh, S.; Ramnath, B.V.; Jayasooriya, M.; Ragavan, R. Review on Mechanical Characteristics of Kevlar Composites. *J. Mines Met. Fuels* **2022**, 387–394. [[CrossRef](#)]
63. Eyvazian, A.; Taghizadeh, S.A.; Hamouda, A.M.; Tarlochan, F.; Moeinifard, M.; Gobbi, M. Buckling and crushing behavior of foam-core hybrid composite sandwich columns under quasi-static edgewise compression. *J. Sandw. Struct. Mater.* **2019**, *23*, 2643–2670. [[CrossRef](#)]
64. Miao, H.; Wu, Z.; Ying, Z.; Hu, X. The numerical and experimental investigation on low-velocity impact response of composite panels: Effect of fabric architecture. *Compos. Struct.* **2019**, *227*, 111343. [[CrossRef](#)]
65. Brod, M.; Dean, A.; Scheffler, S.; Gerendt, C.; Rolfes, R. Numerical modeling and experimental validation of fatigue damage in Cross-Ply CFRP composites under inhomogeneous stress states. *Compos. Part B Eng.* **2020**, *200*, 108050. [[CrossRef](#)]
66. Kumar, P.A.V.; Dean, A.; Reinoso, J.; Paggi, M. A multi phase-field-cohesive zone model for laminated composites: Application to delamination migration. *Compos. Struct.* **2021**, *276*, 114471. [[CrossRef](#)]
67. Dean, A.; Reinoso, J.; Jha, N.; Mahdi, E.; Rolfes, R. A phase field approach for ductile fracture of short fibre reinforced composites. *Theor. Appl. Fract. Mech.* **2020**, *106*, 102495. [[CrossRef](#)]

68. Dean, A.; Kumar, P.A.V.; Reinoso, J.; Gerendt, C.; Paggi, M.; Mahdi, E.; Rolfes, R. A multi phase-field fracture model for long fiber reinforced composites based on the Puck theory of failure. *Compos. Struct.* **2020**, *251*, 112446. [[CrossRef](#)]
69. Dean, A.; Sahraee, S.; Özenc, K.; Reinoso, J.; Rolfes, R.; Kaliske, M. A thermodynamically consistent framework to couple damage and plasticity microplane-based formulations for fracture modeling: Development and algorithmic treatment. *Int. J. Fract.* **2016**, *203*, 115–134. [[CrossRef](#)]

**Disclaimer/Publisher’s Note:** The statements, opinions and data contained in all publications are solely those of the individual author(s) and contributor(s) and not of MDPI and/or the editor(s). MDPI and/or the editor(s) disclaim responsibility for any injury to people or property resulting from any ideas, methods, instructions or products referred to in the content.